



Emitter structure of power heterojunction bipolar transistor for enhancement of thermal stability

J.G. Lee, T.K. Oh, B. Kim, B.K. Kang *

Department of Electrical Engineering, Pohang University of Science and Technology, San 31, Hyoja-Dong, Pohang, Kyungpook 790 784, South Korea

Received 13 April 2000; received in revised form 18 July 2000; accepted 31 August 2000

Abstract

This paper proposes two methods for enhancing thermal stability of a multi-finger power heterojunction bipolar transistor (HBT). The methods adjust either the spacing or length of emitter fingers to improve thermal stability. The temperature rise at the device center of the space-adjusted HBT is suppressed by reducing heat flow from adjacent fingers, and that of the length-adjusted HBT is suppressed by reducing heat generation in the region. A five-finger AlGaAs/GaAs HBT is considered for numerical and experimental investigations. The results show that the method is very effective in enhancing thermal stability; the temperature of the device center is reduced and the power level for thermal regression is increased significantly. When compared with an HBT which has emitter fingers of equal spacing and length, the power level for thermal regression is increased by 34% for the space-adjusted HBT and by 67% for the length-adjusted HBT. © 2001 Published by Elsevier Science Ltd. All rights reserved.

Keywords: Heterojunction bipolar transistor; Thermal stability; Power heterojunction bipolar transistor; Thermal regression

1. Introduction

AlGaAs/GaAs heterojunction bipolar transistors (HBTs) are built on a semi-insulating GaAs substrate. The thermal conductivity of GaAs is approximately 1/3 that of Si. Because of poor thermal conductivity, the operation of an AlGaAs/GaAs HBT at a high power level is limited by its thermal effects. The turn-on voltage of an HBT with a single-finger emitter is reduced when the junction temperature is high. Consequently, the collector current increases with the junction temperature for a given base-emitter voltage V_{BE} . For microwave power applications, most HBTs use an array of emitter fingers to increase the power handling capability. The operating current and voltage of HBT are pushed to the limit to achieve a high power density, and the transistors

operates at an elevated junction temperature. The maximum output power of a multi-finger HBT is limited by the current-gain-collapse phenomenon [1]. This phenomenon occurs when the junction temperature is high. For a multi-finger HBT, the junction temperature of each finger differs because the thermal conductivity of the GaAs substrate is poor. Hotter fingers draw more current than colder fingers and the junction temperature of hotter fingers tend to increase, drawing more current. This type of electro-thermal positive feedback causes the collector current I_C in the common-emitter $I-V$ characteristics to drop suddenly. The collapse loci, the collector current as a function of collector-emitter bias voltage V_{CE} at which the collapse occurs, trace out a curve nearly obeying a constant power law [1].

Many design techniques, such as the use of a thermal shunt [2], a flip-chip bonding structure [3], an emitter ballast resistor [4], and a base ballast resistor [5], have been investigated to increase the power level at which the current-gain-collapse phenomenon occurs. When a thermal shunt or a flip-chip bonding structure is

* Corresponding author. Tel.: +82-562-279-2226; fax: +82-562-279-2903.

E-mail address: bkkang@postech.ac.kr (B.K. Kang).

Nomenclature

| | | | |
|--------|---|----------|--------------------------------------|
| T_0 | temperature of heat-sink (300°K) | J_C | collector current density |
| $k(T)$ | thermal conductivity | J_{C0} | collector saturation current density |
| k_0 | thermal conductivity of GaAs at 300°K | κ | Boltzmann constant |
| L_x | length in x -direction for numerical analysis | η_C | ideality factor |
| L_y | length in y -direction for numerical analysis | δ | electro-thermal feedback constant |
| d | thickness of the substrate | R_{th} | thermal resistance |

adopted, the heat transfer from the active device region to a heat-sink located near the emitter finger is facilitated, resulting in a more uniform temperature distribution between fingers. If a ballast resistor is connected to either the base or emitter, it gives a negative feedback to the base or collector current. The negative feedback reduces the temperature difference between fingers and prevents thermal instability. Along with these methods, the length and spacing of emitter fingers are optimized using an electro-thermal simulation [1,6,7].

Almost all power HBTs reported to the present have emitter fingers of equal length and spacing, as shown in Fig. 1(a). For this structure, the temperature of fingers in the device center rises faster than that of other fingers because the thermal coupling is higher in the device center than in the device periphery. The heated center fingers draw more current and the temperature increases

further. For this reason, as the collector current increases by increasing the base current, the base-emitter voltage increases at a low collector current where the thermal effects are insignificant, but it decreases at a high collector current. The collector current (threshold current) at which the base-emitter voltage begins to decrease is used as a criterion for onset of thermal instability, and this criterion is called the regression criterion [8]. This threshold current can be identified from a I_C-V_{BE} graph (regression loci). After the onset of thermal instability, the current through the peripheral fingers decreases because more current flows through the fingers in the device center. Because of this phenomenon, the temperature of the peripheral fingers decreases although the total power consumption increases (Table 1).

In this paper, two types of emitter structures, which can enhance the thermal properties of a multi-finger HBT, are proposed. The structures of emitter fingers are shown in Fig. 1(b) and (c). The spacing of the emitter finger is adjusted in Fig. 1(b) to reduce heat flow from adjacent fingers to the device center. The length of the emitter finger is adjusted in Fig. 1(c) to reduce the heat generation in the device center. Using a numerical analysis, the spacing and lengths of emitter fingers are determined, and HBTs of these structures are fabricated and measured. An electro-thermal model of HBT and the numerical results are given in Section 2. The HBT fabrication processes and experimental results are given in Section 3, and a conclusion is given in Section 4.

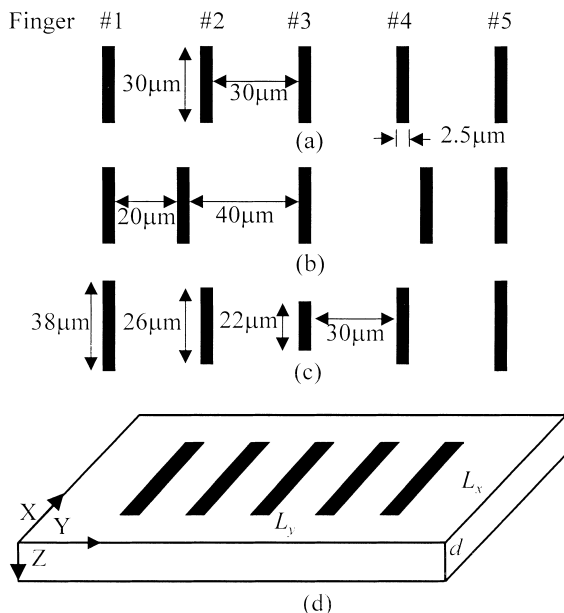


Fig. 1. Structure of emitter fingers for a multi-finger power HBT: (a) reference, (b) space-adjusted, (c) length-adjusted devices and (d) a simple geometrical model of HBT for thermal calculation.

2. Thermal model and numerical analysis

For thermal calculation of HBTs whose emitter finger layouts are shown in Fig. 1(a)–(c), a simple geometrical model shown in Fig. 1(d) is considered. The width of all emitter fingers is $2.5 \mu\text{m}$ and the total device area is kept constant at $375 \mu\text{m}^2$ ($5 \times 2.5 \times 30 \mu\text{m}^2$ for Fig. 1(a) and (b) and $2.5 \times (38 \times 2 + 26 \times 2 + 22) \mu\text{m}^2$ for Fig. 1(c)). For all devices, finger #3 is located at the center and the other fingers are located symmetrically around finger #3. For the reference device (Fig. 1(a)), all emitter fingers have length of $30 \mu\text{m}$ and all spaces between fingers are $30 \mu\text{m}$. The area and thickness, d , of

Table 1
A structure of epitaxial layer for AlGaAs/GaAs HBT

| | Composition | Thickness (μm) | Doping concentration (cm^{-3}) |
|---------------|---|-----------------------------|---|
| Emitter cap | $\text{In}_x\text{Ga}_{1-x}\text{As}$ ($x = 0.5$) | 0.02 | 2.0×10^{19} |
| Buffer | $\text{In}_x\text{Ga}_{1-x}\text{As}$ ($0 \rightarrow 0.5$) | 0.02 | $0.5\text{--}2.0 \times 10^{19}$ |
| Emitter | GaAs | 0.09 | 5.0×10^{18} |
| Emitter | GaAs | 0.07 | 5.0×10^{17} |
| Emitter | $\text{Al}_x\text{Ga}_{1-x}\text{As}$ ($0.3 \rightarrow 0$) | 0.03 | 5.0×10^{17} |
| Emitter | $\text{Al}_x\text{Ga}_{1-x}\text{As}$ ($x = 0.3$) | 0.07 | 5.0×10^{17} |
| Base | GaAs | 0.07 | 5.0×10^{19} |
| Collector | GaAs | 1.0 | 2.0×10^{16} |
| Sub-collector | GaAs | 0.6 | 5.0×10^{18} |

the substrate for numerical analysis are $L_x \times L_y = 300 \times 400 \mu\text{m}^2$ and $100 \mu\text{m}$, respectively.

The structure of each finger is shown in Fig. 2. The emitter is composed of an n^+ -InGaAs layer to improve Ohmic contact, and n-GaAs/AlGaAs layers to form the emitter region. The p^+ -GaAs layer forms the base and the n-GaAs and n-GaAs layers form the collector. During operation, most of the collector current flow through the collector under the intrinsic emitter, and the base-collector junction voltage is close to the emitter-collector voltage. Therefore, it can be assumed that a major heat source is located at the base-collector junction. Because the base-collector junction is located at $0.37 \mu\text{m}$ below the emitter surface, the temperature of emitter surface is very close to the base-collector junction temperature.

The following heat transfer equation is used to calculate the temperature profile:

$$\nabla \cdot k(T)\nabla T = 0 \quad (1)$$

where, $k(T)$ is the thermal conductivity and $T(x, y, z)$ is the temperature at a position (x, y, z) . If all heat sources are located at $z = 0$ plane, the temperature of a heat-sink located at $z = d$ is T_0 , and the heat flows through side walls are neglected, the boundary conditions for Eq. (1) are given by

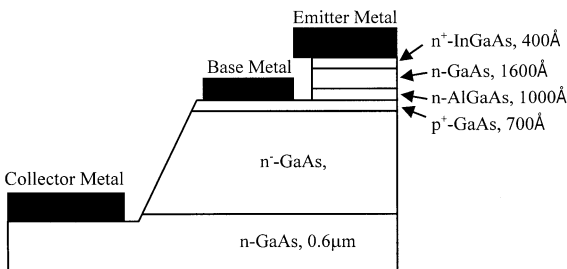


Fig. 2. The structure of an emitter finger for a multi-finger power HBT.

$$\left. \frac{\partial T}{\partial x} \right|_{x=0} = \left. \frac{\partial T}{\partial x} \right|_{x=L_x} = \left. \frac{\partial T}{\partial y} \right|_{y=0} = \left. \frac{\partial T}{\partial y} \right|_{y=L_y} = 0,$$

$$k(T) \left. \frac{\partial T}{\partial z} \right|_{z=0} = -p(x, y, 0),$$

$$T|_{z=d} = T_0,$$

where $p(x, y, 0)$ is the density of power consumed at a point $(x, y, 0)$. Because the thermal conductivity depends on temperature for a semiconductor, the heat transfer equation is nonlinear. The Kirchhoff conversion equation is convenient to solve a nonlinear heat transfer equation [9]. This equation converts a solution of a linear heat transfer equation with a constant thermal conductivity into a solution of the nonlinear equation with a temperature-dependent thermal conductivity. When the temperature dependency of the thermal conductivity is given by [10]

$$k(T) = k_0 \left(\frac{T}{T_0} \right)^{-b}, \quad (2)$$

the Kirchhoff's equation

$$\theta = T_0 + \frac{1}{k_0} \int_{T_0}^T k(T) dT$$

gives the following relation between the actual temperature $T(x, y, z)$ and the temperature $\theta(x, y, z)$ obtained by putting $k(T) = k(T_0) \equiv k_0$:

$$T = \left[\frac{1}{T_0^{b-1}} - \frac{(b-1)(\theta - T_0)}{T_0^b} \right]^{-1/(b-1)}. \quad (3)$$

The constant b is 1.22 for GaAs.

For numerical analysis, the top surface of the structure given in Fig. 1(d) is divided into cells having an area of $\Delta x \times \Delta y = 1 \times 1.25 \mu\text{m}^2$. If the thermal conductivity is independent on temperature, the solution θ for Eq. (1) at the top surface is given by [1]

$$\theta(x, y, 0) = T_0 + \sum_{i=1}^N \left(\frac{p_i d\Delta x \Delta y}{L_x L_y k_0} + \sum_{m,n=0}^{\infty} K_{mn} \cos \frac{m\pi x}{L_x} \cos \frac{n\pi y}{L_y} \right), \quad (4)$$

where, $p_i \Delta x \Delta y$ is the heat generated in the i th cell at (x_i, y_i) , N is the total number of cells, m and n are integers, the constants K_{mn} are defined as

$$K_{mn} \equiv \frac{C_{mn} p_i}{k_0 \gamma_{mn}} \cos \frac{m\pi x_i}{L_x} \cos \frac{n\pi y_i}{L_y} \tanh(\gamma_{mn} d),$$

$$\gamma_{mn} = \pi \sqrt{\left(\frac{m}{L_x}\right)^2 + \left(\frac{n}{L_y}\right)^2},$$

$$C_{mn} = \begin{cases} \frac{16}{m\pi^2} \sin \frac{m\pi \Delta x}{2L_x} \sin \frac{n\pi \Delta y}{2L_y} & \text{for } m \neq 0, n \neq 0, \\ \frac{4\Delta y}{m\pi L_y} \sin \frac{m\pi \Delta x}{2L_x} & \text{for } m \neq 0, n = 0, \\ \frac{4\Delta x}{n\pi L_x} \sin \frac{n\pi \Delta y}{2L_y} & \text{for } m = 0, n \neq 0, \end{cases}$$

The solution for the nonlinear heat-transfer Eq. (1) is obtained after inserting Eq. (4) into Eq. (3). However, the dependency of collector current on temperature should be given to determine the heat generated by each finger. A single-finger HBT, which has the structure shown in Fig. 2, has been fabricated and its collector current versus base-emitter voltage characteristics are measured at a temperature range of 300–450°K with a step of 25°K. Using the measured data, the dependency of collector current on temperature are obtained with the following equation for collector current density J_C [11]:

$$J_C = J_{C0} \exp\left(\frac{V_{BE} - J_C R_E + \delta(T - T_0)}{\eta_C \kappa T_0 / q}\right) \quad (5)$$

where J_{C0} is the collector saturation current density, κ is the Boltzman constant, $\eta_C \approx 1.1026$ is the ideality factor, R_E is the electrical resistance per unit area of the emitter, and $\delta \equiv -\partial V_{BE} / \partial T$ reflects the decrease in V_{BE} due to a temperature increase. The experimental constants J_{C0} , R_E , and δ are extracted from the Gummel plots (J_C versus V_{BE} plots) at different temperature.

For numerical calculation, it is assumed initially that the collector current I_C is distributed evenly to all fingers and each fingers dissipates the same amount of power. The initial profile of temperature is calculated by solving Eq. (1), and corrections to J_C for each finger are made subsequently using Eq. (5). While calculating J_C , V_{BE} is adjusted to give the same total collector current I_C . After calculation of J_C , a new temperature profile is obtained using

$$p(x, y, 0) = J_C(x, y) V_{CE}$$

which is the power density at each cell. These steps are iterated until the changes in temperatures of every cell are less than 0.1°K, and the final J_C and temperature profile are obtained.

Using the above procedure, the lengths and spaces of fingers are optimized. For the space-adjusted device (Fig. 1(b)), all fingers have the same length of 30 μm , and the first (between fingers #1 and 2) and the last spaces are 20 μm , while the center spaces are 40 μm . For the length-adjusted device (Fig. 1(c)), all the spaces between fingers are 30 μm , but the lengths of fingers are 22 μm for finger #3, 26 μm for fingers #2 and 4, and 38 μm for fingers #1 and 5. For all devices, the total area of emitter fingers is 375 μm^2 and the distance between the device center and outermost finger is kept constant to 62.5 μm .

The peak temperature versus power consumption P_{DC} is shown in Fig. 3. For the reference device (filled square), the peak temperature increases rapidly after $P_{DC} = 235$ mW and it becomes 450°K at $P_{DC} = 260$ mW. The space-adjusted (filled circle) and length-adjusted (filled triangle) devices have the peak temperature of 400°K and 380°K, respectively, although P_{DC} is increased to 280 mW. These results indicate that the space-adjusted and length-adjusted devices have better thermal stability than the reference device. The reason can be understood from Fig. 4, which shows the temperature of each finger at a given P_{DC} . At $P_{DC} = 110$ mW (open marks), the differences in temperature between fingers are small. When P_{DC} increases to 260 mW (filled marks), the average temperature increases for all devices. However, the space-adjusted fingers, and length-adjusted devices show small temperature differences between fingers. The difference in temperature for the reference

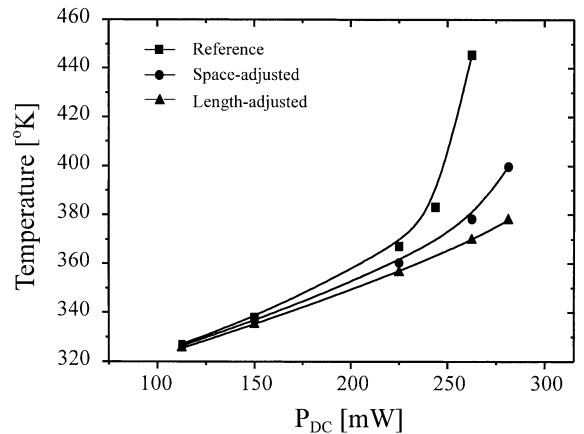


Fig. 3. Peak temperature versus power consumption for the reference (■), space-adjusted (●), and length-adjusted (▲) devices.

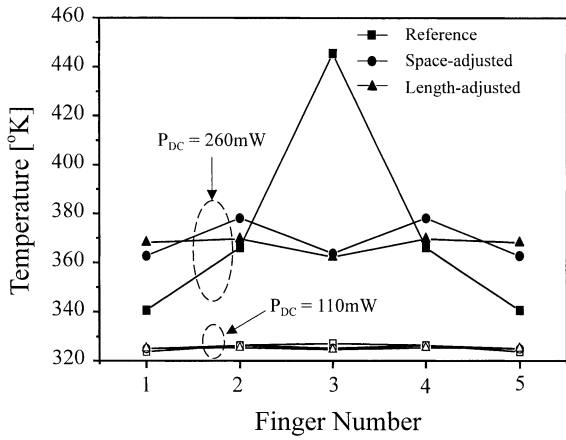


Fig. 4. Temperature of each finger at $P_{DC} = 110$ mW (\square , \circ , Δ) and $P_{DC} = 260$ mW (\blacksquare , \bullet , \blacktriangle) for the reference (\square , \blacksquare), space-adjusted (\circ , \bullet), and length-adjusted (Δ , \blacktriangle) devices.

device is approximately 110°K, while those for the length-adjusted and space-adjusted devices are 8°K and 16°K, respectively. Because of the heat flow from adjacent fingers, the temperature of the center finger for the reference device is much higher than that of the other fingers. For the space-adjusted device, the heat flow from adjacent fingers to the center finger is reduced by increasing the spacing between fingers. For the length-adjusted device, the power consumption at the device center is reduced by using short fingers. The temperatures of fingers #1 and 2 of the reference device at $P_{DC} = 260$ mW are 340.5°K and 366°K, respectively. They increase to 347.2°K and 368.7°K when P_{DC} reduces to 240 mW (not shown in Fig. 4). These observations indicate that the current flow at $P_{DC} = 260$ mW is concentrated to the center finger and the temperature of the center finger is high enough to induce thermal instability.

3. Experimental results

An epitaxial layer for device fabrication are given in Table 1. It was grown on a semi-insulating (100) GaAs wafer. The emitter consists of a 200 Å thick $n^+-\text{In}_{0.5}\text{Ga}_{0.5}\text{As}$ emitter cap layer with doping concentration of 2×10^{19} cm^{-3} , a 200 Å thick $n^+-\text{In}_x\text{Ga}_{1-x}\text{As}$ ($x = 0.5 \rightarrow 0$) graded layer with a doping concentration of $5 \times 10^{18} - 2 \times 10^{19}$ cm^{-3} , a 900 Å thick $n^+-\text{GaAs}$ and a 700 Å thick $n\text{-GaAs}$ emitter buffer layer with doping concentrations of 5×10^{17} cm^{-3} , and a 700 Å thick $n\text{-Al}_{0.3}\text{Ga}_{0.7}\text{As}$ layer with a doping concentration of 5×10^{17} cm^{-3} . The 700 Å thick $p^+-\text{GaAs}$ base layer with a doping concentration 5×10^{19} cm^{-3} and a sheet resistivity of 240 Ω/square . The collector consists of a 1 μm

thick $n\text{-GaAs}$ layer with a doping concentration of 2×10^{16} cm^{-3} and a 6000 Å thick $n^+-\text{GaAs}$ sub-collector layer with a doping concentration of 5×10^{18} cm^{-3} .

The wet-etching chemicals are an H_2SO_4 solution for GaAs and InGaAs etching and $\text{K}_2\text{Cr}_2\text{O}_7:\text{H}_3\text{PO}_4:\text{H}_2\text{O} = 0.625 \text{ g}:150 \text{ ml}:157.6 \text{ ml}$ solution for AlGaAs/GaAs selective etching. The InGaAs layer was wet etched with the emitter electrode as a mask, and the GaAs emitter layer was dry-etched selectively using CCL_2F_2 plasma. The etch selectivity of GaAs with respect to AlGaAs was better than 100:1. For self-alignment of the base metal, an undercut of ~ 0.2 μm was formed over-etching of the GaAs layer. The AlGaAs layer was wet etched after deposition of a Si_3N_4 layer to protect the InGaAs layer. After etching of the AlGaAs layer, a self-aligned base metal was deposited. The GaAs collector layers were wet etched using an H_2SO_4 solution, and the collector metal was deposited. The semi-insulating GaAs substrate was wet etched for device isolation. After isolation etching, a Si_3N_4 passivation layer was deposited over the entire active area. The base electrode was connected to a base pad using Au over the Si_3N_4 layer, and the emitter electrode was connected to the emitter pad using an air bridge. The contact metals were a 1300/400/1600 Å thick AuGe/Ni/Au layer for the n-type emitter and collector, and a 400/400/1000 Å thick Ti/Pt/Au layer for the p-type base. To prevent etching of the Au layer during RIE process, a 100 Å thick Cr layer was deposited on the surface of the emitter electrode. The alloy condition for ohmic contacts was 400°C for 20 s in N_2 ambience.

To check the thermal properties of the fabricated HBTs, the thermal resistance and regression loci are measured. The thermal resistance defined by the following equation shows the rate of increase of the junction temperature with the power consumption [12]:

$$R_{th} \equiv \frac{(1/\delta)\Delta V_{BE}}{I_C \Delta V_{CE}} \quad (6)$$

Here, ΔV_{BE} and ΔV_{CE} represent changes in V_{BE} and V_{CE} when P_{DC} changes, while keeping I_C constant. The electro-thermal feedback constant δ depends on J_C , and its value is $\sim 1.4 \text{ mV}^\circ\text{K}^{-1}$ for $J_C = 10^3 \text{ A cm}^{-2}$ and $\sim 1.2 \text{ mV}^\circ\text{K}^{-1}$ for $J_C = 10^4 \text{ A cm}^{-2}$ [13]. The measured V_{BE} of the reference device for $V_{CE} = 4 \text{ V}$ and $I_C = 40 \text{ mA}$, which corresponds to $J_C = 1.1 \times 10^4 \text{ A cm}^{-2}$ and $\delta \approx 1.2 \text{ mV}^\circ\text{K}^{-1}$, is 1.5178 V. When V_{CE} increases to 6 V, while keeping $I_C = 40 \text{ mA}$, V_{BE} decreases to 1.4851 V, resulting in $R_{th} = 340.6^\circ\text{K W}^{-1}$. The thermal resistances measured at the same conditions are $286.4^\circ\text{K W}^{-1}$ and $284.4^\circ\text{K W}^{-1}$ for the space-adjusted and length-adjusted devices, respectively. These values correspond to 15.9% and 16.8% improvement on R_{th} when compared to the reference device.

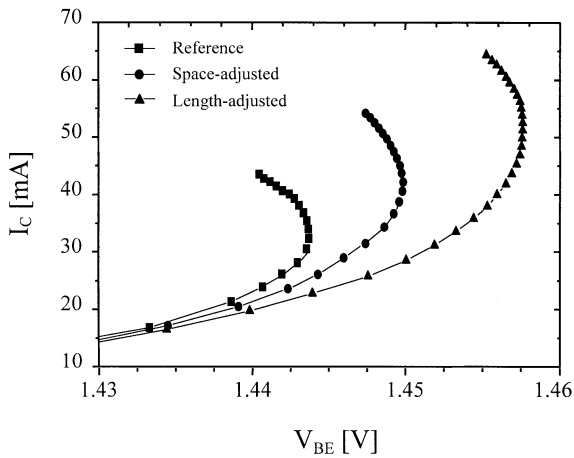


Fig. 5. The regression loci measured at $V_{CE} = 8$ V for the reference (■), space-adjusted (●), and length-adjusted (▲) devices.

When V_{CE} changes from 6 to 8 V, while keeping $I_C = 40$ mA, the reference, space-adjusted, and length-adjusted devices have ΔV_{BE} of 0.043, 0.0306 and 0.0304 V, respectively. The corresponding R_{th} s are 448°K W^{-1} , $318.7^\circ\text{K W}^{-1}$, and $316.7^\circ\text{K W}^{-1}$. When compared with R_{th} s measured at $V_{CE} = 4$ –6 V, the R_{th} s for the space-adjusted and length-adjusted devices increase a little at $V_{CE} = 6$ –8 V, while that for the reference device increases significantly. The improvements on R_{th} s at $V_{CE} = 6$ –8 V for the space-adjusted and length-adjusted devices are 28.9% and 29.3% of that for the reference device, respectively.

The regression loci are measured at $V_{CE} = 8$ V and shown in Fig. 5. The thermal collapse occurs at $I_C = 32$ mA and $P_{DC} = 256$ mW for the reference device, $I_C = 43$ mA and $P_{DC} = 344$ mW for the space-adjusted device, and $I_C = 53$ mA and $P_{DC} = 424$ mW for the length-adjusted device. The base-emitter voltages at the regression point are 1.4437, 1.4497, and 1.4574 V for the reference, space-adjusted, and length-adjusted devices, respectively. The power levels at which the thermal collapse occurs on the space-adjusted and length-adjusted devices are 34% and 67% higher than that on the reference device.

4. Conclusions

To alleviate the thermal regression problems in a multi-finger power HBT, two types of emitter structures are proposed; one has a space-adjusted finger structure and the other has a length-adjusted finger structure. For the space-adjusted device, the heat flow from adjacent fingers to the center finger is reduced by increasing the spacing between fingers. For the length-adjusted device, the heat generation at the device center is reduced by

using short fingers. From numerical results for five-finger HBTs, it is shown that the temperature difference between fingers of the proposed devices is much lower than that of a reference device, which have emitter fingers of equal length and spacing. The proposed devices are fabricated and their thermal properties are measured. When compared with the reference device, the thermal resistances of the space-adjusted and length-adjusted devices are improved by 28.9% and 29.3%, respectively. The power level of the space-adjusted and length-adjusted devices for thermal regression is increased by 34% and 67%, respectively. These results indicate that the proposed structures are very useful for improving the thermal properties of a power HBT.

Acknowledgements

This work was supported by Korea Agency for Defense Development and by Ministry of Education under BK21 project. A part of HBT fabrication process was performed at Samsung Advanced Institute of Technology.

References

- [1] Liou LL, Bayraktaroglu B. Thermal stability analysis of AlGaAs/GaAs heterojunction bipolar transistors with multiple emitter fingers. *IEEE Trans Electron Dev* 1994;41:629–36.
- [2] Sewell S, Liou LL, Barlage D, Barrette J, Bozada C, Dettmer R, Fitch F, Jenkins T, Lee R, Mack M, Trombley G, Watson P. Thermal characterization of thermally-shunted heterojunction bipolar transistors. *IEEE Electron Dev Lett* 1996;17:19–21.
- [3] Jenkins T, Bozada C, Dettmer R, Sewell J, Via D, Barrette J, Ebel J, Desalvo G, Havasy C, Liou L, Quach T, Gillespie J, Pettiford C, Ito C, Nakano K, Anholt R. Comparison of thermal-shunt and flip-chip HBT thermal impedance: comment on novel HBT with reduced thermal impedance. *IEEE Microwave Guided Wave Lett* 1996;6:268–9.
- [4] Gao G, Selim B, Unlu M, Morkoc H, Blackburn DL. Emitter ballasting resistor design for, and current handling capability of AlGaAs/GaAs power heterojunction bipolar transistors. *IEEE Trans Electron Dev* 1991;38:185–96.
- [5] Liu W, Khatibzadeh A, Sweder J, Chau HF. The use of base ballasting to prevent the collapse of current gain in AlGaAs/GaAs heterojunction bipolar transistor. *IEEE Trans Electron Dev* 1996;43:245–51.
- [6] Zhou W, Sheu S, Liou JJ, Huang CI. A multi-emitter finger AlGaAs/GaAs HBT model including the effects of two-dimensional temperature distribution on emitter fingers. *Solid-State Electron* 1998;42:693–8.
- [7] Ihn B, Kim MS, Kim WN, Lee JG, Park KS, Chung MC, Oh TK, Kang BK, Kim B. Design and fabrication of X-band AlGaAs/GaAs power HBTs. *Asia Pacific Microwave Conference*. 1997. p. 1113–6.

- [8] Liu W, Khatibzadeh A. The collapse of current gain in multi-finger heterojunction bipolar transistors: its substrate temperature dependence, instability criteria, and modeling. *IEEE Trans Electron Dev* 1994;41:1698–707.
- [9] Joyce WB. Thermal resistance of heat sinks with temperature-dependent conductivity. *Solid-State Electron* 1975; 18:321–2.
- [10] Maycock PD. Thermal conductivity of silicon, germanium, III–V compounds and III–V alloys. *Solid-State Electron* 1967;10:161–8.
- [11] Ihn B, Kim B. A highly accurate Gummel plot model for thermal design of high-power microwave HBTs. *Microwave Optical Tech Lett* 1997;16:12–5.
- [12] Liu W, Nelson S, Hill DG, Khatibzadeh A. Current gain collapse in microwave multifinger heterojunction bipolar transistors operated at very high power densities. *IEEE Trans Electron Dev* 1994;40:1917–27.
- [13] Liu W, Yuksel A. A survey of thermal-electric feedback coefficient in GaAs-based heterojunction bipolar transistors. *Solid-State Electron* 1995;38:407–11.